Published in final edited form as:
Cancer Res. 2014 September 1; 74(17): 4937–4945. doi:10.1158/0008-5472.CAN-14-1042.

Live-cell imaging of invasion and intravasation in an artificial microvessel platform

Andrew D. Wong[1,2] and **Peter C. Searson**[1,2]

[1] Department of Materials Science and Engineering, Johns Hopkins University, 3400 North Charles Street, Baltimore, MD 21218, USA

[2] Institute for Nanobiotechnology Johns Hopkins University, 3400 North Charles Street, Baltimore, MD 21218

Abstract

Methods to visualize metastasis exist, but additional tools to better define the biological and physical processes underlying invasion and intravasation are still needed. One difficulty in studying metastasis stems from the complexity of the interface between the tumor microenvironment and the vascular system. Here we report the development of an investigational platform that positions tumor cells next to an artificial vessel embedded in an extracellular matrix (ECM). On this platform, we used live-cell fluorescence microscopy to analyze the complex interplay between metastatic cancer cells and a functional artificial microvessel which was lined with endothelial cells. The platform recapitulated known interactions, and its use demonstrated the capabilities for a systematic study of novel physical and biological parameters involved in invasion and intravasation. In summary, our work offers an important new tool to advance knowledge about metastasis and candidate anti-metastatic therapies.

Keywords

intravasation; metastasis; tumor microenvironment; breast cancer; tumor vasculature

INTRODUCTION

Metastasis is a complex, multistep process responsible for more than 90% of cancer-related deaths (1), and yet there remain many unanswered questions concerning the steps in the metastatic cascade (2). Critical steps, such as invasion, intravasation, and extravasation, take place at or near the interface between the tumor microenvironment and the vascular system (2, 3), which plays a significant role in modulating tumor growth and progression (4, 5).

Correspondence should be addressed to Peter C. Searson (searson@jhu.edu) Peter C. Searson 120 Croft Hall, 3400 N Charles ST, Baltimore, MD 21218 Phone: (410) 516-8774 Fax: (410) 516-2355.

AUTHOR CONTRIBUTIONS

ADW and PCS designed the experiments. ADW performed the experiments. ADW and PCS analyzed the data and wrote the paper.

COMPETING FINANCIAL INTERESTS

The authors declare no competing financial interests.

Supplementary Information is available in the online version of this paper.

While the development of 3D extracellular matrix (ECM) platforms have contributed to advances in the study of invasion (6, 7), there are currently no platforms that combine ECM with a physiologically relevant vessel for the study of intravasation and extravasation. Similarly, *in vivo* models are widely employed in cancer research, but it is difficult to study the intermediate steps in the metastatic cascade. An *in vitro* model that can recapitulate the complex physical and biochemical interplay between tumor cells, the vascular system, and the surrounding ECM may have significant impact on our understanding of tumor progression.

Adapting an approach from vascular engineering, we have developed a platform that allows us to form a perfusable artificial vessel comprised of endothelial cells within a type I collagen matrix (8). By incorporating both single and clusters of MDA-MB-231 breast cancer cells (BCCs) in the ECM around the vessel, we recapitulate many features of the distinct tumor niche within a microenvironment encompassing the vascular system. Here, we use live-cell fluorescence microscopy to monitor the interactions between the BCCs, vessel endothelium, and ECM and compare them to our current understanding of invasion, intravasation, and angiogenesis. This novel tumor/ECM/vessel platform provides a new approach to investigate the physical and biochemical changes during the progression of cancer to discover important insights in metastasis and provide the basis for new therapeutic approaches.

MATERIALS AND METHODS

Fabricating a perfusable cylindrical ECM scaffold

The ECM/vessel platform is comprised of a cylindrical collagen channel located within a polydimethylsiloxane (PDMS) housing that is perfused by a gravity flow system (Fig. 1A). An aluminum mold with 3 rectangular channels of dimension 1.2 mm × 1.5 mm × 5 cm (W × H × L) was used to form the housing by casting PDMS (Fig. 1B). After removal from the mold, holes are punched for connections to tubing and reservoirs, and the PDMS housing is plasma bonded to a glass slide. A custom nozzle, 1.6 mm in diameter and 1 cm in length, is inserted into each rectangular compartment to guide the insertion of the template rod and to direct flow into the channel during perfusion (Fig. 1C). The interior of the PDMS housing is silanized with (3-glycidyloxypropyl)trimethoxysilane (Sigma-Aldrich, St. Louis, MO) to improve adhesion of the subsequently introduced collagen gel. Prior to collagen introduction, devices and flow setups were sterilized by autoclaving. High concentration rat tail type I collagen (BD Biosciences, San Jose, CA) is used to form the ECM with the manufacture's recommended neutralizing protocol using 1N NaOH, 10x PBS, and distilled water. Collagen is the main structural protein within the body; types I, III, and IV are constitutively present in normal mammary glands and increasingly within the stroma of neoplastic mammary tissue and invasive carcinoma (9). Type I collagen was used to form a hydrogel scaffold that best represents the structural, biochemical, and transport properties of *in vivo* tumor tissue and permits both cellular adhesion and remodeling to facilitate endothelial vessel formation and tumor cell migration. Here we use a collagen density of 7 mg ml^{-1} resulting in a matrix stiffness of about 200 Pa (10). The ECM can be formed at lower gel concentrations although maintaining higher shear stresses becomes more difficult.

A cancer cell suspension was introduced immediately after neutralizing the collagen solution to obtain a final concentration of 5×10^5 cells ml^{-1}. Neutralized collagen solutions were injected into the rectangular channels. Nitinol rods (McMaster-Carr, Princeton, NJ) of 150 μm in diameter were threaded through the nozzles and into the collagen solution to be used as cylindrical templates for collagen casting. During collagen neutralization and injection, all solutions and devices were kept on ice. Optically transparent collagen gels were formed by incubating the device at 37 °C during initial gelation for 15 min and allowed to complete gelation at room temperature for 1 h. Template rods were slowly removed, leaving behind a cylindrical channel (Fig. 1C). Endothelial cells were introduced into the channels at a concentration of 10^6 ml^{-1}. Channels typically yielded 50,000 cells cm^{-2} of coverage after seeding and would be confluent within 24 h. After forming a microvessel, the device is placed under steady laminar flow using an automatically recirculating gravity flow system. The device is kept under hydrostatic pressure of 10 cm of water with a height difference of about 5 cm between the upper and lower reservoirs (Fig. 1D). Vessels were maintained at a shear stress of 12 - 15 dyne cm^{-2}. During multiple day live-cell imaging experiments, both the device and the reservoirs are contained within separate chambers in the microscope incubator and maintained at 37 °C under constant humidity and 5% CO_2 (Fig. 1E). Most devices were overrun by proliferating tumor cells after 1 - 2 weeks of culture.

Cell lines and culture conditions

Dual-labeled MDA-MB-231 adenocarcinoma and HT-1080 fibrosarcoma cells (AntiCancer Inc., San Diego, CA) were cultured in RPMI (Corning Inc) supplemented with 10% fetal bovine serum (FBS) (Life Technologies), and 1% penicillin/streptomycin (Life Technologies) at physiological conditions (humidified 37 °C with 5% CO_2). Human umbilical vein endothelial cells (HUVEC) (PromoCell, Heidelberg, Germany) and adult human dermal microvascular endothelial cells (HMVEC) (Life Technologies) were cultured using EGM-2 (PromoCell) growth media with all supplementary ingredients: 2% fetal calf serum, hydrocortisone, heparin, ascorbic acid, hEGF, hVEGF, hbFGF, and R3 IGF-1. All cell lines were authenticated by their respective manufacturers and tested negative for mycoplasm.

Live-cell fluorescence imaging

Time-lapse, phase-contrast, and fluorescence images were captured using automated image acquisition software from Nikon with a TE-2000 U microscope (Fig. 1E) (Nikon Instruments Inc., Melville, NY). A 10× objective was used for all epifluorescence and phase-contrast imaging. Confocal z-stacks were obtained on a LSM 710 with a 20× water immersion objective (N.A. = 1.0) (Carl Zeiss, Oberkochen, Germany) from which 3D and cross-sectional projections of the stacks were obtained using LSM Image Browser (Carl Zeiss).

Quantifying vessel permeability

Permeability was measured through quantitative fluorescence detection of molecular transport from inside the vessel to the surrounding ECM (8, 11, 12). Bovine serum albumin (BSA) conjugated to Alexa Fluor 488 (Life Technologies, Carlsbad , CA) at 5 μg ml^{-1} was introduced into the vessels and imaged every 2 min. Image intensity profiles were obtained

using ImageJ (NIH, Bethesa, MD) and permeability coefficients were calculated by extracting the initial step increase in fluorescence on introducing BSA into the vessel lumen and the slope corresponding to the rate of permeation from the vessel to the ECM (Fig. 2F).

Image analysis of tumor/endothelial interactions

Time-lapse videos of merged fluorescence and phase-contrast images were imported into ImageJ as stacks of TIFF files. The invasion front of a cluster of breast cancer cells (BCCs) was measured by manually tracing its perimeter using phase-contrast images, from which shape factor and tortuosity were extracted. The motility of single dual-labeled BCCs was quantified by selecting the approximate center of each GFP expressing nucleus and measuring its change in distance at 12 min intervals. For tracking individual endothelial cells, each cell was manually traced in phase-contrast images (Supplementary Video S8), and its respective centroid position was calculated. To obtain the relative distance between a sprouting endothelial cell's protrusions and an adjacent tumor, the difference between the y-value of the tip's position and a reference point behind the tumor was taken and plotted vs. time (Fig. 4A); the tip of each endothelial protrusion was manually selected from phase-contrast images. The same operation was used to obtain the difference between the centroid positions of neighboring endothelial cells with an adjacent tumor.

Particle image velocimetry (PIV) analysis

PIV analysis of endothelial monolayers within the collagen channels was conducted in MATLAB using OpenPIV (13). Time-lapse phase-contrast images obtained at 10 min intervals were imported into OpenPIV as TIFF files with a resolution of 0.64 μm px^{-1}. Monolayers of endothelial cells in focus on the bottom or top of the collagen channels were selected as regions of interest. A 16x16 px area was used for both the interrogation window and spacing/overlap. Batch means of the velocity magnitudes of each vector in the 2D field were obtain from the unfiltered OpenPIV output.

Statistical Analysis

Values are represented as mean ± s.e.m. The principle statistical test used was a t-test (two-tailed with unequal variance). We considered a P-value less than 0.05 to be statistically significant.

RESULTS AND DISCUSSION

Characterizing the ECM/vessel platform for studying invasion and intravasation

The ECM/vessel platform is comprised of a cylindrical channel lined with a confluent monolayer of endothelial cells in a collagen type I matrix located within a PDMS housing and perfused at a shear stress of 12-15 dyne cm^{-2} by a gravity flow system (Fig. 1). Figure 1 is described in more detail in Materials and Methods. For experiments reported here, our vessels are lined with either human dermal microvascular endothelial cells (HMVECs) or human umbilical vein endothelial cells (HUVECs). Dual-labeled MDA-MB-231 BCCs (GFP histone tag, RFP cytoplasm) or RFP-expressing HT-1080 fibrosarcoma cells (14) are embedded within the collagen matrix as either single cells or clusters. Phase-contrast movies of the top and bottom of the microvessels were used to characterize the endothelium

(Supplementary Video S1; Fig. 2A). Immunofluorescence images were obtained by sequentially introducing reagents and antibodies directly into the vessel (Fig. 2B). Scanning electron microscope (SEM) images of the collagen matrix show uniform 100 nm diameter collagen fibers, typical of higher gelation temperatures (15) (Fig. 2C). A cross-section of a confocal z-stack shows a cylindrical vessel within the collagen matrix with approximately 15 endothelial cells around the perimeter (Fig. 2D). High resolution z-stack images of the vessels were obtained by removing the bulk collagen gel from the PDMS housing and using a water immersion objective for imaging. A projection of a confocal z-stack shows a vessel formed from HUVECs with multiple HT-1080 fibrosarcoma cells in the ECM extending protrusions towards the vessel wall (Fig. 2E; Supplementary Fig. S1).

Permeability measurements were used to assess endothelial monolayer integrity and barrier function (Fig. 2F). HUVEC vessels exhibited slightly lower permeabilities to fluorescently-labeled BSA ($4.3 \pm 1.2 \times 10^{-7}$ cm s^{-1}) compared to HMVEC vessels ($2.7 \pm 0.6 \times 10^{-6}$ cm s^{-1}) (Fig. 2G). Vessels with BSA permeabilities $< 5 \times 10^{-6}$ cm s^{-1} were generally stable for longer than 1 week. Particle image velocimetry (PIV) was used to analyze phase-contrast movies of endothelial monolayers and to assess overall vessel activity. HUVEC monolayers were less active than HMVEC monolayers with an average PIV speed about 40% lower (Fig. 2H).

Invasion

MDA-MB-231 BCCs degrade the local ECM, allowing them to move rapidly within etched out tracks in the matrix. Figure 3A shows a series of time-lapse images of two BCCs that have degraded the local ECM resulting in a narrow tunnel approximately 300 μm in length. Both BCCs move rapidly back and forth at speeds up to 1.1 μm min^{-1} and occasionally make contact with the endothelium (Supplementary Video S2). From hours 4 to 8, one of the BCCs extends a protrusion into the interface directly between the endothelium and the ECM. While it is unable to fully insert itself into the interface, its motility is temporarily reduced until it withdraws the protrusion from the ECM/vessel interface after 12 hours. Despite degradation of the underlying substrate, the endothelium bridges the etched region and effectively encloses the BCC within the tunnel.

These observations are consistent with the current understanding of tumor cell invasion and migration. Highly directed migration can occur along large fibers in low density ECM networks (16) or along predefined matrix tunnels that confine cell migration (17-19). Since our gels are relatively dense, we observe the latter case where rapid protease-independent motility of tumor cells occurs along preexisting tracks made by previously migrating tumor cells or individual 'leader' cells that have been shown to generate the initial tracks and align collagen fibers along these paths of least mechanical resistance (19). Tunnels can also be formed by fibroblasts, endothelial cells, and smooth muscle cells (17, 18) and may be used by tumor cells as protease-independent, high speed networks that facilitate collective tumor migration (18, 19) (Supplementary Video S3). When BCCs make contact with blood vessels in mouse models, migration slows abruptly; this has been attributed to increased ECM density around the vessel wall resulting in slower amoeboid movement (16). We similarly

observe slower migration of BCCs at the ECM/vessel interface possibly due to the stabilization of protrusions within the interface.

Chemotactic gradients within the tumor microenvironment may promote the migration of cancer cells towards blood vessels (4, 20, 21). In Figure 3B, we show a series of time-lapse images of a single BCC that begins approximately 100 μm from the vessel wall and migrates towards the endothelium with high directedness (d = 0.8; net path/total path), an average speed of 0.3 μm min^{-1}, and a maximum speed of 1.0 μm min^{-1} (Supplementary Video S4). During invasion, the BCC extends multiple protrusions from its leading edge (noticeable at 5 h) towards the vessel. Upon approaching the endothelium (at 10 h), the leading protrusions pull the cell body down separate tracks in the ECM, and cell motility decreases as its body is wrapped around a blocking fiber. The invasion of the single BCC reflects our current understanding of tumor cell migration through dense ECM by proteolytic degradation during amoeboid migration (7, 16). The single BCC exhibits an extended, polarized cell body under tension with a rounded trailing edge lacking a tail. Stable polarization of actin polymerization at the tumor cell's leading edge may be regulated by chemokine gradients, such as EGF (16, 22) supplied by the circulating growth media, and angiocrine factors released locally by the vessel endothelium, such as bFGF, G-CSF, and CXCL8 (4). The cell's relatively high, sustained invasion speed also suggests loosely attached focal complexes. As described above, after 48 h, the cell body and nucleus deforms around an obstacle as the leading protrusions continue to pull the cell towards the vessel wall. At 72 h the BCC's protrusions extend farther into the interface; however, the cell is held in place by the blocking fiber. This may be because the cell was unable to fully degrade the ECM during the time period of the experiment. By using less dense collagen concentrations and gelling at lower temperatures, the ECM stiffness can be reduced and pore sizes increased to enhance BCC invasion. Additionally, the stabilization of multiple leading edge protrusions at the ECM/vessel interface may prevent their retraction, thus holding the tumor cell in place. When cells are able to retract their protrusions, they may proceed to invade down a single track into the interface and subsequently intravasate (Supplementary Video S5).

Types of behavior at the ECM/vessel interface

When BCCs approach the vessel wall, we observe a variety of tumor-endothelium interactions, including (1) inactive BCCs that dwell at the ECM/vessel interface, (2) activated BCCs that intravasate, and (3) clusters of BCCs that promote localized vessel sprouts. Here, we describe these tumor-endothelium interactions in the context of our current understanding of tumor cell dormancy, intravasation, and sprouting angiogenesis.

Tumor cell dormancy

During assembly of the platform, single BCCs embedded at the ECM/vessel interface (Fig. 3C) often remain as single cells that do not proliferate. The net distance travelled by these cells is 19.4 ± 11 μm in 24 h (n = 3). In contrast, BCCs along the inside of bare collagen channels with no endothelium travel 155 ± 47 μm in 24 h (n = 9). The reduced motility of cancer cells along endothelial lined vessels may be attributed to confinement at the ECM/vessel interface. Cancer cell motility depends on the formation of new focal adhesions in the direction of migration and dissociation at the trailing edge (7); however, competition with

endothelial cells for substrate surface area may limit their ability to extend filopodia. The reduced proliferation and motility of BCCs at the interface may also be regulated by the expression of quiescence-inducing angiocrine factors by the endothelium (5, 23). In cell culture, endothelial cells have been shown to modify their substrates through the secretion of basement membrane proteins (24). For example, the deposition of perlecan, heparin and thrombospondin-1, have been shown to reduce cancer cell invasion and proliferation leading to tumor cell dormancy (5, 23, 25). Endothelial modification of the microenvironment may play a significant role in regulating tumor cell activity and dispersal.

Intravasation

Intravasation of a tumor cell requires local disruption of the endothelial junctions (26, 27). In the tumor vasculature a partially activated endothelium with detached and depleted pericytes is likely to facilitate transendothelial migration (28). Figure 3D shows a series of time-lapse images of a single BCC moving along the interface between the ECM and the endothelium. The average velocity along the interface is 0.17 μm min^{-1}, but at 13 h, the BCC halts, loses polarity, and rounds up as proximal endothelial cells become activated and extend protrusions into the ECM at 14.3 h. As the cell contracts, the endothelium is displaced and the BCC is directly exposed to shear stress as its body protrudes approximately 50 μm into the vessel. At 15 h, the BCC is carried away by flow after detaching an active portion of its RFP-expressing cytoplasm in the collagen ECM. At the site of intravasation, the monolayer is disrupted, exhibiting a 200 μm gap where a local endothelial cell divides (Supplementary Video S6). Within 24 h after intravasation, the endothelial monolayer has reformed over the exposed defect and the remaining tumor cytoplasm has been degraded (Fig. 3D). In contrast to the tumor cell quiescence described above, in this case we observe a single BCC that locally activates the endothelium, as seen by the resulting endothelial extension of filopodia 30 μm into the ECM around the BCC. BCCs are known to secrete a variety of mitogenic factors and cytokines that locally activate endothelial cells (20). In addition to biochemical activation, the single tumor cell was able to mechanically deform the endothelium by contracting into a sphere and exerting a protrusive force into the vessel. This contraction may be caused by mitosis, during which disassembly of focal adhesions and actin cytoskeletal reorganization results in cell rounding, cortical stiffening, and a sharp increase in cell height (29) (Supplementary Fig. S2). This combination of biochemical activation and mechanical protrusion may have contributed to the disruption of the endothelial cell junctions, resulting in exposure of the BCC to shear stress prior to its detachment and escape into the vessel.

Figure 3E shows a series of images of a cluster of BCCs located approximately 100 μm from the endothelial monolayer taken at 5 day intervals. Due to the relatively high density and stiffness of the collagen ECM, invasion occurs by proteolytic degradation of the ECM through the expression of MMPs (7). At day 1, the tumor is approximately spherical with a shape factor of 0.85. By day 5, the shape factor has decreased to 0.40 and the perimeter of the tumor facing the vessel is 30% more tortuous than the opposite side and reaches 50% by day 10. At day 15, the tumor growth is biased towards the vessel, growing 30% faster on the vessel facing side, as single BCCs initiate matrix degradation along the periphery. By day 20, the tumor has increased to 27-times its original size; however, tumor cells do not occupy

the space in the center of the tumor where an empty volume of degraded ECM exists. The lack of BCCs at the center of the tumor suggests that invasion is not driven by proliferation, but by proteolytic degradation. The biased growth of the BCCs towards the vessel may be due to growth factor gradients created by the perfused media or the endothelium. EGF within the media is a strong chemoattractant, shown to increase MDA-MB-231 directional motility, but not proliferation (30). Despite the enhanced migration towards the vessel, single BCCs do not make contact with the endothelium. EGF may be attracting tumor cells to the vessel, but the endothelium may be expressing repulsive guidance cues, such as Slit2, that locally repel tumor cells (31).

Angiogenesis

Paracrine signaling between tumor cells and endothelial cells has been shown to initiate the formation of endothelial sprouts (32). In Figure 3F, we show a series of time-lapse images of a cluster of BCCs within 30 μm of the vessel wall. The growing cluster of tumor cells extends invadapodia that exert tension on the peripheral ECM; the collagen fibers transduce this mechanical stress which distorts the vessel wall such that it bulges towards the tumor. Over the 6 h period, the endothelial cell closest to the tumor extends protrusions that fluctuate in length between 15 and 20 μm and come within 2 to 5 μm of similar protrusions from the BCCs. While the closest endothelial cell extends protrusions that oscillate in length with a period of about 4 h, its neighboring ECs remain inactive within the monolayer over the lifetime of the protrusions (Supplementary Video S7 and S8). These observations are consistent with the current understanding of the initiation of tumor angiogenesis, which typically begins with the activation of local endothelial cells in response to a chemotactic gradient originating from tumor cells (20). In a non-saturating, chemotactic gradient, the endothelium will exhibit a regulated angiogenic response where usually a single tip cell is followed by neighboring stalk and quiescent phalanx cells (33, 34). The tip cell extends filopodia in the direction of the gradient and secretes MMPs in order to degrade the local ECM (34). Over a period of 24 h, we see modulation of the activated cell's filopodia, but do not see subsequent stalk and phalanx cell formation. While we observe an initial angiogenic response, there may not be enough chemotactic driving force from the BCCs to encourage further development of an angiogenic sprout. Additionally, the matrix may be sufficiently stiff such that it limits the invasion of angiogenic sprouts over the duration of the experiment (10).

While we do not see the formation of stalk and phalanx cells, the activated cell appears to mechanically influence the displacement of its neighboring endothelial cells. Over a 14 hour period, the activity of the sprouting cell's two tips appear to be correlated with their lengths oscillating approximately in phase with a periodicity of about 4 h (Fig. 4A; Supplementary Video S8). The fluctuating tips on the activated cell induce oscillations in the centroid position of the left near neighbor cell, which moves up and down in phase with the tips. However, the forces generated by the activated cell do not appear to be transmitted to the second near neighbor cells (Fig. 4A). There are noticeable protrusions extending from the adjacent tumor towards the activated cell, but because they are largely out of focus, it is unclear if they exhibit coordinated movement with the activated cell's protrusions.

Tumor and endothelium characterization

Several matricellular glycoproteins and proteoglycans secreted by endothelial cells, such as thrombospondin-1 (TSP-1), laminin, and perlecan, have been shown to inhibit the proliferation and invasion of tumor cells (5, 23). Monolayers of HMVEC cells cultured on glass deposit TSP-1 between the substrate and endothelial monolayer (Fig. 4B). The presence of TSP-1 between the vessel endothelium and the collagen ECM may contribute to the reduced activity of single BCCs at the interface through the induction of quiescence and tumor cell dormancy (5) (Fig. 3C). In addition to biochemical suppression of activity, the endothelium may be mechanically impeding the spread of BCCs at the interface. BCCs migrating along the interface exhibit 40% reduced speed compared to migration within predefined ECM tracks (Fig. 4C). While the presence of endothelial cells impedes the speed of BCCs, interface migration is 60% faster than invasion within bulk ECM, which requires proteolytic degradation. This is consistent with *in vivo* observations of tumor cells achieving greater dispersal along secondary structures such as blood and lymphatic vessels (28, 35).

We have developed a platform to mimic the tumor microenvironment based on a confluent monolayer of endothelial cells in a cylindrical geometry and embedded in an extracellular matrix. This is similar to the tumor vasculature which lacks many features of normal blood vessels, such as a well-defined layer of smooth muscle cells and pericytes (28, 36, 37). We apply physiologically relevant shear stress on the vessel, which has been shown to influence paracrine signaling between tumor cells and the endothelium (38). The tumor microenvironment usually exhibits poor lymphatic drainage, and hence our platform does not incorporate transmural pressure and interstitial flow (37); however, these fluid forces have been shown to regulate tumor invasion and vessel sprouting and can be included through the addition of drainage ports along the channel (39, 40). Despite the lack of these features of normal vasculature, the dense collagen ECM and cylindrical architecture supports the formation of a well-defined vessel while promoting tumor growth and invasion through a matrix of biologically and tumor relevant ECM protein (41). ECM properties such as stiffness, pore size, fiber alignment, and composition are expected to influence invasion and intravasation of cancer cells (21, 41) and may be systematically altered within the device.

A variety of tumor/endothelium interactions have been observed by incorporating MDA-MB-231 BCCs within the ECM/vessel platform. Signaling between the tumor and endothelium may be transduced through soluble cytokine and growth factor gradients as well as non-soluble factors deposited during matrix remodeling (Fig. 4D). For example, soluble angiocrine factors such as bFGF, G-CSF, and CXCL8 among others may direct tumor cells towards the vessel endothelium through chemotactic gradients (4, 20); however, thrombospondin-1 (TSP-1) deposited by the endothelium, in addition to laminin, collagen IV, and perlecan, may contribute to the locally reduced activity of BCCs at the interface (5, 23). Meanwhile, tumor cells are known to secrete angiogenic factors such as VEGF, CXCL1, and CXCL8 (20) that compete with the quiescence signaling of the vasculature. We provide a summary of these interactions (Fig. 4D), several of which are consistent with our observations within the platform and have been previously characterized as hallmarks of metastasis, such as invasion, intravasation, angiogenesis, and tumor cell dormancy (37).

Intravasation has been less well studied and until now has been largely limited to *in vivo* observations and 2D *in vitro* assays lacking physiological shear stress and a relevant geometry (16, 26, 27). Here we image tumor cells embedded in the matrix around a 3D cylindrical vessel under flow; however, our method could be extended to investigate the role of other cells involved in the metastatic cascade by incorporating tumor associated macrophages, fibroblasts, and myeloid derived suppressor cells (20). This will be important for understanding the complex role of inflammation and cytokines associated with cancer, which can be difficult to isolate *in vivo* (Fig. 4D). In addition to loading cells within the ECM, we can introduce them through the vessel to study hemodynamic effects on the interactions between circulating tumor cells and the endothelium leading to extravasation. Furthermore, the platform can be used to explore the complex pharmacokinetics and efficacy of systemically delivered drugs.

Until now, the lack of technologies for direct control over physical and biochemical factors influencing tumor-vessel interactions has been a major limiting factor in the investigation of metastasis. A clearer understanding of these interactions at the tumor/ECM/vessel interface will provide new and important insights into the progression of cancer and may provide the basis for new therapeutic approaches.

Supplementary Material

Refer to Web version on PubMed Central for supplementary material.

Acknowledgments

GRANT SUPPORT

The authors gratefully acknowledge support from National Institutes of Health (NIH R01CA170629).

Financial support: NCI Provocative Questions (NIH R01CA170629)

REFERENCES

1. Fidler IJ. Timeline - The pathogenesis of cancer metastasis: the ‘seed and soil’ hypothesis revisited. Nat Rev Cancer. 2003; 3:453–8. [PubMed: 12778135]
2. Chambers AF, Groom AC, MacDonald IC. Dissemination and growth of cancer cells in metastatic sites. Nat Rev Cancer. 2002; 2:563–72. [PubMed: 12154349]
3. Steeg PS. Tumor metastasis: mechanistic insights and clinical challenges. Nat Med. 2006; 12:895–904. [PubMed: 16892035]
4. Butler JM, Kobayashi H, Rafii S. Instructive role of the vascular niche in promoting tumour growth and tissue repair by angiocrine factors. Nat Rev Cancer. 2010; 10:138–46. [PubMed: 20094048]
5. Ghajar CM, Peinado H, Mori H, Matei IR, Evason KJ, Brazier H, et al. The perivascular niche regulates breast tumour dormancy. Nat Cell Biol. 2013; 15:807–17. [PubMed: 23728425]
6. Fraley SI, Feng Y, Krishnamurthy R, Kim DH, Celedon A, Longmore GD, et al. A distinctive role for focal adhesion proteins in three-dimensional cell motility. Nat Cell Biol. 2010; 12:598–604. [PubMed: 20473295]
7. Friedl P, Wolf K. Tumour-cell invasion and migration: Diversity and escape mechanisms. Nat Rev Cancer. 2003; 3:362–74. [PubMed: 12724734]
8. Chrobak KM, Potter DR, Tien J. Formation of perfused, functional microvascular tubes in vitro. Microvasc Res. 2006; 71:185–96. [PubMed: 16600313]

9. Lagace R, Grimaud JA, Schurch W, Seemayer TA. Myofibroblastic stromal reaction in carcinoma of the breast: variations of collagenous matrix and structural glycoproteins. Virchows Arch A Pathol Anat Histopathol. 1985; 408:49–59. [PubMed: 3933171]
10. Cross VL, Zheng Y, Won Choi N, Verbridge SS, Sutermaster BA, Bonassar LJ, et al. Dense type I collagen matrices that support cellular remodeling and microfabrication for studies of tumor angiogenesis and vasculogenesis in vitro. Biomaterials. 2010; 31:8596–607. [PubMed: 20727585]
11. Yuan Y, Chilian WM, Granger HJ, Zawieja DC. Permeability to albumin in isolated coronary venules. Am J Physiol. 1993; 265:H543–52. [PubMed: 8368358]
12. Huxley VH, Curry FE, Adamson RH. Quantitative fluorescence microscopy on single capillaries: alpha-lactalbumin transport. Am J Physiol. 1987; 252:H188–97. [PubMed: 3492924]
13. Taylor ZJ, Gurka R, Kopp GA, Liberzon A. Long-duration time-resolved piv to study unsteady aerodynamics. IEEE T Instrum Meas. 2010; 59:3262–9.
14. Hoffman RM. The multiple uses of fluorescent proteins to visualize cancer in vivo. Nat Rev Cancer. 2005; 5:796–806. [PubMed: 16195751]
15. Raub CB, Suresh V, Krasieva T, Lyubovitsky J, Mih JD, Putnam AJ, et al. Noninvasive assessment of collagen gel microstructure and mechanics using multiphoton microscopy. Biophys J. 2007; 92:2212–22. [PubMed: 17172303]
16. Condeelis J, Segall JE. Intravital imaging of cell movement in tumours. Nat Rev Cancer. 2003; 3:921–30. [PubMed: 14737122]
17. Gaggioli C, Hooper S, Hidalgo-Carcedo C, Grosse R, Marshall JF, Harrington K, et al. Fibroblast-led collective invasion of carcinoma cells with differing roles for RhoGTPases in leading and following cells. Nat Cell Biol. 2007; 9:1392–U92. [PubMed: 18037882]
18. Sabeh F, Shimizu-Hirota R, Weiss SJ. Protease-dependent versus -independent cancer cell invasion programs: three-dimensional amoeboid movement revisited. J Cell Biol. 2009; 185:11–9. [PubMed: 19332889]
19. Wolf K, Wu YI, Liu Y, Geiger J, Tam E, Overall C, et al. Multi-step pericellular proteolysis controls the transition from individual to collective cancer cell invasion. Nat Cell Biol. 2007; 9:893–904. [PubMed: 17618273]
20. Roussos ET, Condeelis JS, Patsialou A. Chemotaxis in cancer. Nat Rev Cancer. 2011; 11:573–87. [PubMed: 21779009]
21. Brabek J, Mierke CT, Rosel D, Vesely P, Fabry B. The role of the tissue microenvironment in the regulation of cancer cell motility and invasion. Cell Commun Signal. 2010; 8:22. [PubMed: 20822526]
22. Bailly M, Yan L, Whitesides GM, Condeelis JS, Segall JE. Regulation of protrusion shape and adhesion to the substratum during chemotactic responses of mammalian carcinoma cells. Exp Cell Res. 1998; 241:285–99. [PubMed: 9637770]
23. Franses JW, Baker AB, Chitalia VC, Edelman ER. Stromal endothelial cells directly influence cancer progression. Sci Transl Med. 2011; 3:66ra5.
24. Huber AR, Weiss SJ. Disruption of the subendothelial basement membrane during neutrophil diapedesis in an in vitro construct of a blood vessel wall. J Clin Invest. 1989; 83:1122–36. [PubMed: 2703527]
25. Iozzo RV, Sanderson RD. Proteoglycans in cancer biology, tumour microenvironment and angiogenesis. J Cell Mol Med. 2011; 15:1013–31. [PubMed: 21155971]
26. Zervantonakis IK, Hughes-Alford SK, Charest JL, Condeelis JS, Gertler FB, Kamm RD. Three-dimensional microfluidic model for tumor cell intravasation and endothelial barrier function. Proc Natl Acad Sci U S A. 2012; 109:13515–20. [PubMed: 22869695]
27. Lee TH, Avraham HK, Jiang S, Avraham S. Vascular endothelial growth factor modulates the transendothelial migration of MDA-MB-231 breast cancer cells through regulation of brain microvascular endothelial cell permeability. J Biol Chem. 2003; 278:5277–84. [PubMed: 12446667]
28. Gerhardt H, Semb H. Pericytes: gatekeepers in tumour cell metastasis? J Mol Med (Berl). 2008; 86:135–44. [PubMed: 17891366]
29. Matzke R, Jacobson K, Radmacher M. Direct, high-resolution measurement of furrow stiffening during division of adherent cells. Nat Cell Biol. 2001; 3:607–10. [PubMed: 11389447]

30. Price JT, Tiganis T, Agarwal A, Djakiew D, Thompson EW. Epidermal growth factor promotes MDA-MB-231 breast cancer cell migration through a phosphatidylinositol 3'-kinase and phospholipase C-dependent mechanism. Cancer Res. 1999; 59:5475–8. [PubMed: 10554021]

31. Brantley-Sieders DM, Dunaway CM, Rao M, Short S, Hwang Y, Gao Y, et al. Angiocrine factors modulate tumor proliferation and motility through EphA2 repression of Slit2 tumor suppressor function in endothelium. Cancer Res. 2011; 71:976–87. [PubMed: 21148069]

32. Chung S, Sudo R, Mack PJ, Wan CR, Vickerman V, Kamm RD. Cell migration into scaffolds under co-culture conditions in a microfluidic platform. Lab Chip. 2009; 9:269–75. [PubMed: 19107284]

33. Hellstrom M, Phng LK, Hofmann JJ, Wallgard E, Coultas L, Lindblom P, et al. Dll4 signalling through Notch1 regulates formation of tip cells during angiogenesis. Nature. 2007; 445:776–80. [PubMed: 17259973]

34. De Smet F, Segura I, De Bock K, Hohensinner PJ, Carmeliet P. Mechanisms of vessel branching: filopodia on endothelial tip cells lead the way. Arterioscler Thromb Vasc Biol. 2009; 29:639–49. [PubMed: 19265031]

35. Burden-Gulley SM, Qutaish MQ, Sullivant KE, Lu H, Wang J, Craig SE, et al. Novel cryo-imaging of the glioma tumor microenvironment reveals migration and dispersal pathways in vivid three-dimensional detail. Cancer Res. 2011; 71:5932–40. [PubMed: 21862632]

36. Baluk P, Hashizume H, McDonald DM. Cellular abnormalities of blood vessels as targets in cancer. Curr Opin Genet Dev. 2005; 15:102–11. [PubMed: 15661540]

37. Hanahan D, Weinberg RA. Hallmarks of cancer: the next generation. Cell. 2011; 144:646–74. [PubMed: 21376230]

38. Buchanan CF, Voigt EE, Szot CS, Freeman JW, Vlachos PP, Rylander MN. Three-dimensional microfluidic collagen hydrogels for investigating flow-mediated tumor-endothelial signaling and vascular organization. Tissue Eng Part C Methods. 2014; 20:64–75. [PubMed: 23730946]

39. Shieh AC, Swartz MA. Regulation of tumor invasion by interstitial fluid flow. Phys Biol. 2011; 8:015012. [PubMed: 21301060]

40. Song JW, Munn LL. Fluid forces control endothelial sprouting. Proc Natl Acad Sci U S A. 2011; 108:15342–7. [PubMed: 21876168]

41. Provenzano PP, Inman DR, Eliceiri KW, Knittel JG, Yan L, Rueden CT, et al. Collagen density promotes mammary tumor initiation and progression. BMC Med. 2008; 6:11. [PubMed: 18442412]

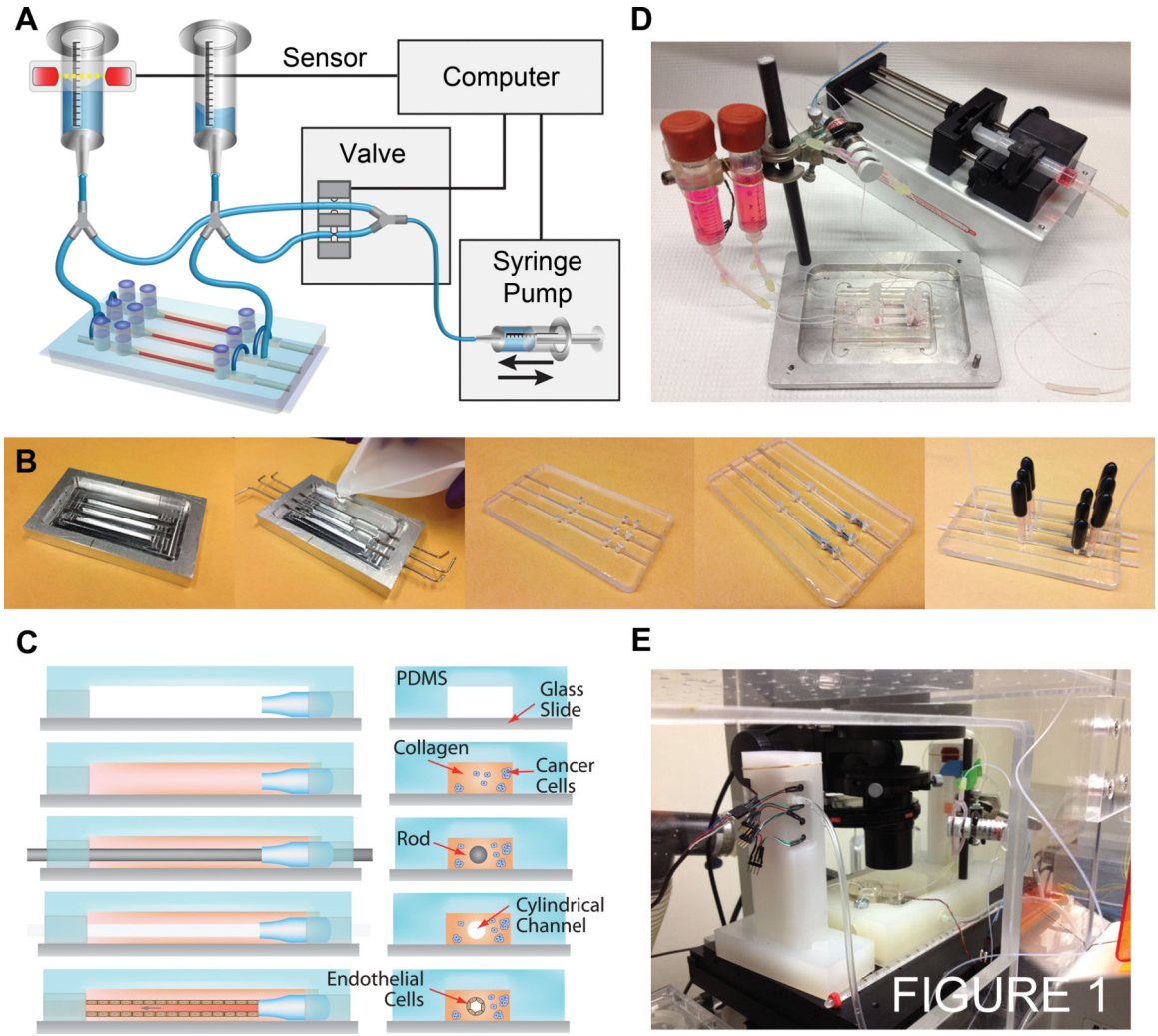

Figure 1.

Design and fabrication of an ECM/vessel platform. A, experimental setup. Gravity flow driven by differential pressure perfuses device. Flow is recycled from the bottom to the top reservoir using a solenoid valve to switch pump and withdraw action. The liquid level is monitored using a break-beam sensor on the top reservoir. B, steps in device fabrication. C, steps in cylindrical channel and collagen ECM fabrication. D, fully assembled device. E, live-cell fluorescence imaging setup.

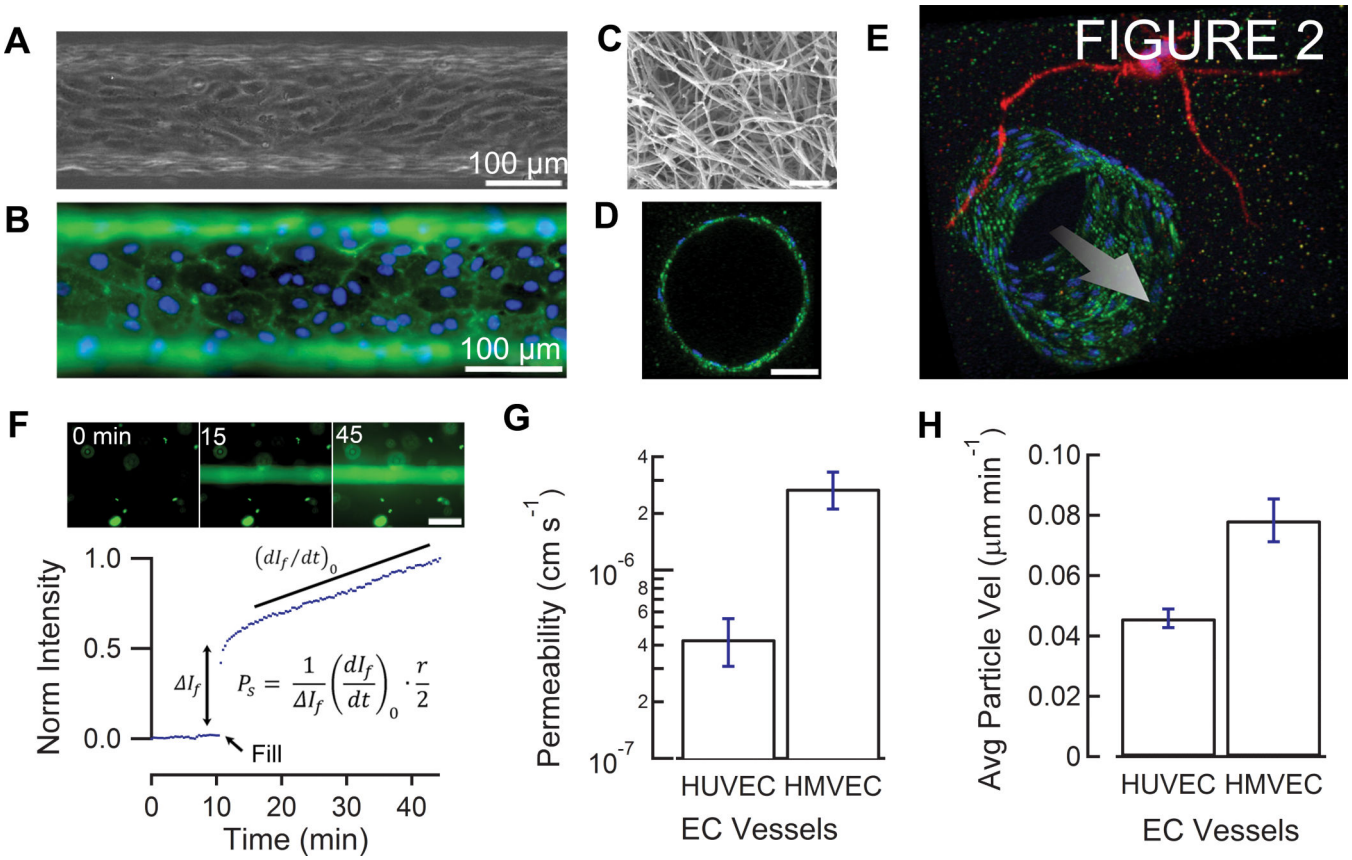

Figure 2.

ECM/vessel characterization. A, phase-contrast image of HUVEC-lined channel. B, immunofluorescence image of PECAM-1 stained HUVEC channel. C, SEM image of collagen matrix. Scale bar, 1 μm. D, cross-section of a confocal z-stack of PECAM-1 (green) stained HUVEC endothelium with DAPI nuclei (blue). Scale bar, 50 μm. E, 3D projection of a confocal z-stack of a PECAM-1 (green) stained HUVEC channel with 2 separate RFP (red) expressing HT-1080 fibrosarcoma cells (red) extending protrusions near the vessel. Nuclei are stained with DAPI (blue). Arrow represents the direction of flow. F, representative fluorescence permeability measurement. Scale bar, 200 μm. G, permeability analysis of HUVEC (n = 4) and HMVEC (n = 4) channels. Error bars represent s.e.m. $P < 0.05$ by unpaired t-test. H, particle image velocimetry (PIV) analysis of HUVEC (n = 3) and HMVEC (n = 2) channels. Error bars represent s.e.m. $P < 0.05$ by unpaired t-test.

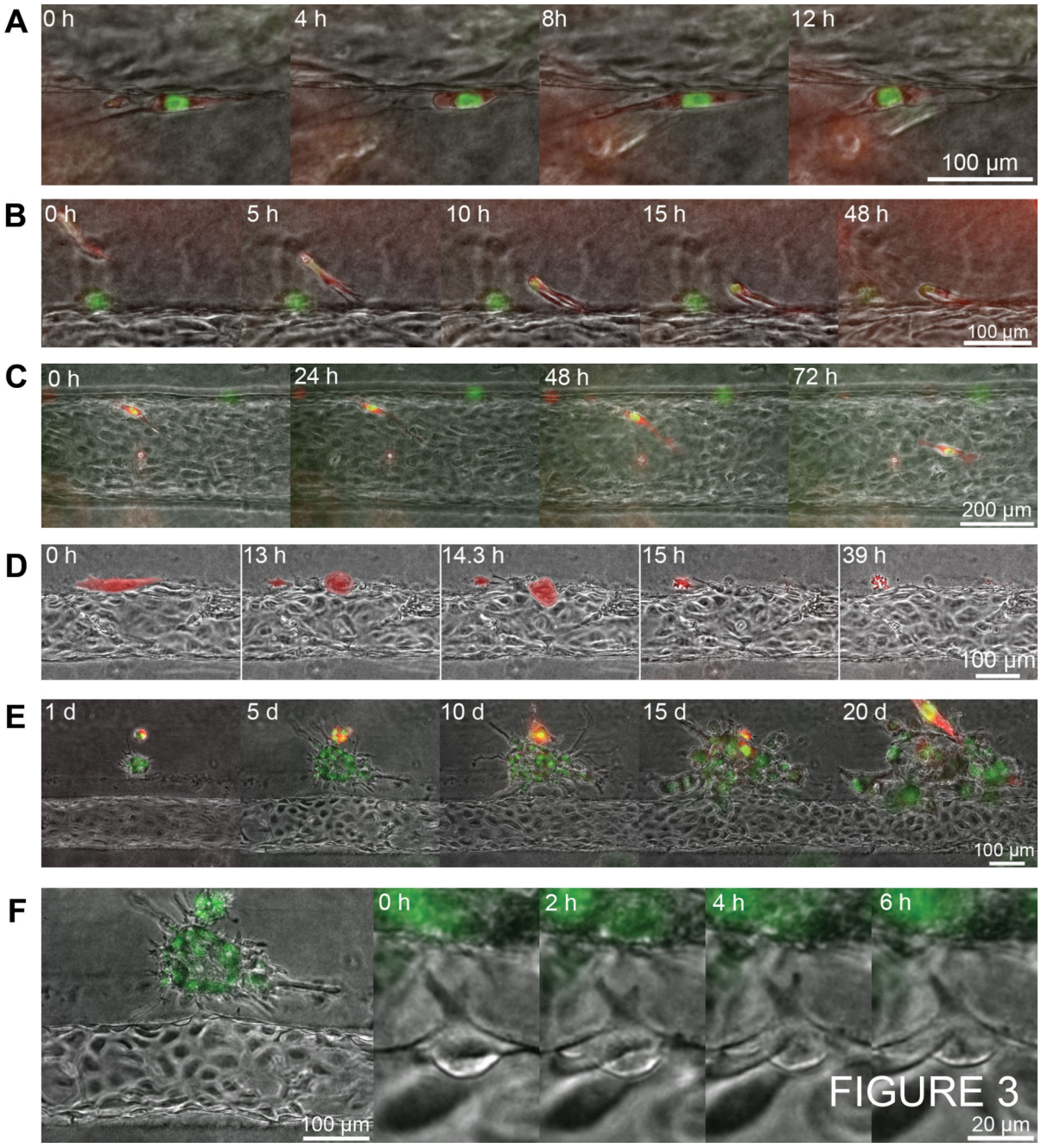

Figure 3.

Time-lapse series of tumor-endothelium-ECM interactions. All vessels are lined with HMVEC and interact with dual-labeled MDA-MB-231 BCCs (GFP nuclei and RFP cytoplasm). A, proteolytic degradation and formation of a matrix tunnel at the interface between the vessel endothelium and ECM. BCC motility is often confined within these regions of unrestricting ECM. B, single BCC invasion through the ECM. C, images of a single BCC at the interface between the endothelium and ECM. D, single BCC intravasation. The BCC is highlighted in red for convenience. E, daily images of a cluster of BCCs adjacent to vessel. F, endothelial cell activation near a cluster of BCCs.

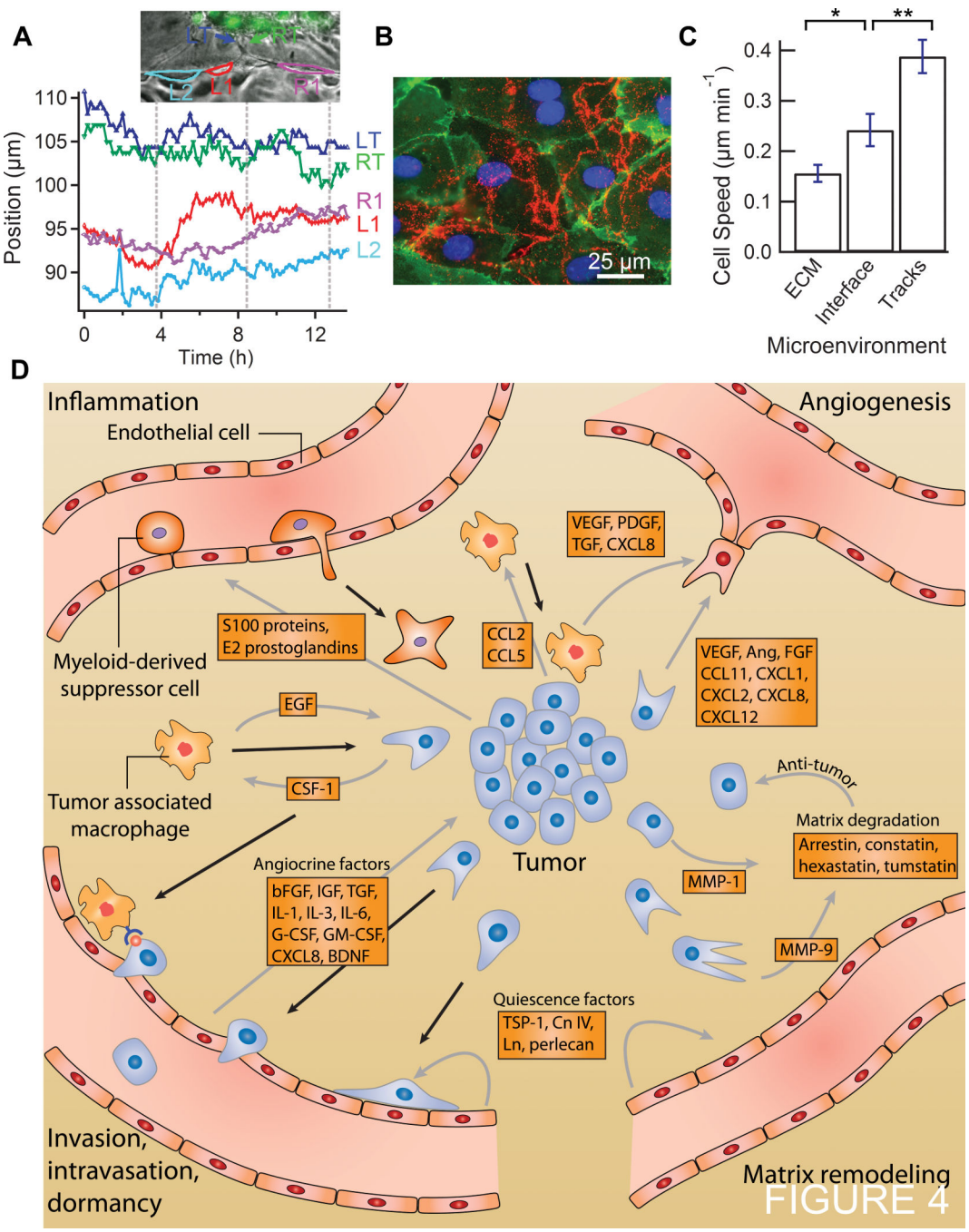

Figure 4.

Characterizing tumor-endothelium interactions. A, tip position and relative cell centroid positions vs. time of an endothelial sprout towards a cluster of MDA-MB-231 BCCs. Vertical dashed lines delineate approximate periods of tip cell oscillations. Abbreviations: left tip (LT), right tip (RT), right neighboring cell (R1), left neighboring cell (L1), second left neighboring cell (L2). B, immunofluorescence image of PECAM-1 (green), DAPI nuclei (blue), and TSP-1 (red) secreted by HMVEC on a glass bottom surface. C, migration speeds (measured over ≥ 12 h) of single BCCs within the collagen ECM (n = 13), predefined matrix

tunnels (n = 23), and the ECM/vessel interface (n = 9). Error bars represent s.e.m. *P < 0.05; **P < 0.01 by unpaired t-test. D, illustration of biochemical signaling pathways and gradients between endothelial cells, tumor cells, tumor associated macrophages, and myeloid-derived suppressor cells. Solid black arrows represent migration. Grey arrows represent chemical gradients.